
SeTAR: Out-of-Distribution Detection with Selective Low-Rank Approximation

Yixia Li^{1*} Boya Xiong^{2*} Guanhua Chen¹ Yun Chen²

¹Southern University of Science and Technology

²Shanghai University of Finance and Economics

liyixia@me.com xiongboya@163.sufe.edu.cn

chengh3@sustech.edu.cn yunchen@sufe.edu.cn

Abstract

Out-of-distribution (OOD) detection is crucial for the safe deployment of neural networks. Existing CLIP-based approaches perform OOD detection by devising novel scoring functions or sophisticated fine-tuning methods. In this work, we propose SeTAR, a novel, training-free OOD detection method that leverages selective low-rank approximation of weight matrices in vision-language and vision-only models. SeTAR enhances OOD detection via post-hoc modification of the model’s weight matrices using a simple greedy search algorithm. Based on SeTAR, we further propose SeTAR+FT, a fine-tuning extension optimizing model performance for OOD detection tasks. Extensive evaluations on ImageNet1K and Pascal-VOC benchmarks show SeTAR’s superior performance, reducing the false positive rate by up to 18.95% and 36.80% compared to zero-shot and fine-tuning baselines. Ablation studies further validate our approach’s effectiveness, robustness, and generalizability across different model backbones.

1 Introduction

The task of out-of-distribution (OOD) detection (Hendrycks & Gimpel, 2017; Ming et al., 2022) aims to identify whether input data comes from an unknown distribution. It has garnered significant attention in the machine learning community recently (Hendrycks et al., 2020; Xu et al., 2021; Miyai et al., 2023a). While machine learning models are trained with supervised in-distribution (ID) data, they often struggle to generalize to OOD data encountered in real-world applications (Emmott et al., 2016) like autonomous vehicles and healthcare. These OOD samples pose challenges as they are not represented in the training data. Consequently, OOD detection plays a crucial role in developing reliable and trustworthy machine-learning models suitable for real-world deployment (Bai et al., 2023). It allows models to filter out and reject these awkward inputs effectively, and enables the use of curated and labeled OOD samples to further train for a more robust model in the wild.

Previous research has primarily focused on detecting OOD instances in either visual (DeVries & Taylor, 2018; Hendrycks & Gimpel, 2017; Liang et al., 2018; Hendrycks et al., 2022) or textual data (Hu & Khan, 2021; Zheng et al., 2020; Zhou et al., 2021; Tan et al., 2019). Recently, significant progress has been made in multimodal tasks like multimodal retrieval (Li et al., 2023; Caesar et al., 2018) and image classification (Yu et al., 2022), thanks to vision-and-language pretrained (VLP) models like CLIP (Radford et al., 2021). More recent studies have explored OOD detection with CLIP, grouped into zero-shot methods (Fort et al., 2021; Ming et al., 2022; Miyai et al., 2023b) and finetuning-based methods (Ming & Li, 2023; Tao et al., 2023; Miyai et al., 2023a). However, the zero-shot methods suffer from suboptimal performance due to potential domain gaps with ID

* Equal Contribution.

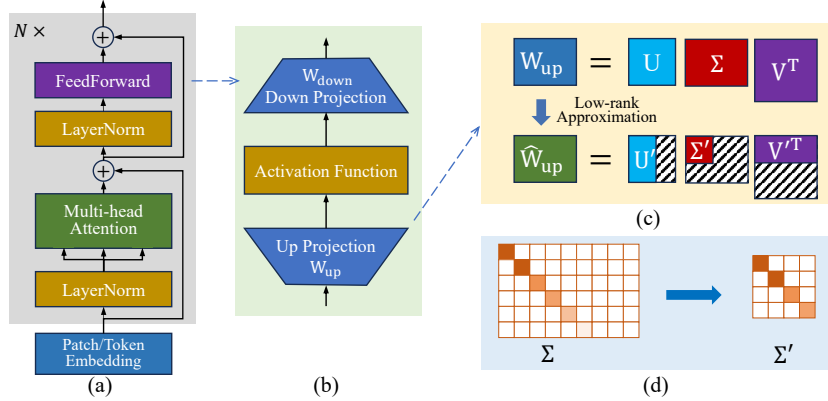


Figure 1: The overview of SeTAR. (a) The structure of the CLIP image and text encoder. (b) The details of the feed-forward sublayer. (c) For each encoder layer, we replace the W_{up} weight matrix with its low-rank approximation \widehat{W}_{up} . (d) The illustration of Σ before and after low-rank approximation. More details are in Section 3.1.

downstream data. On the other hand, finetuning-based methods carry the risk of deconstructing the intricate representations learned by CLIP which requires a meticulously designed training strategy.

In this work, we propose SeTAR, a training-free and effective OOD detection method by selective low-rank approximations. Low-rank approximation is to approximate a given matrix by finding a lower-rank matrix that closely resembles the original matrix. Previous research has demonstrated that using low-rank approximation matrices can achieve comparable performance to full parameters in various scenarios, as observed in tasks such as large language model (LLM) fine-tuning (Hu et al., 2022) and model pruning (Hajimolahoseini et al., 2021). These approaches typically preserve the same rank across different low-rank approximation matrices. In our work, we demonstrate that it is possible to significantly enhance the performance of OOD detection by selectively manipulating the weight matrices in the CLIP model, including the choice of weight matrices and the ratio of singular vectors to be reduced. Specifically, we propose a simple top-to-bottom and image-to-text greedy search algorithm to manipulate W_{up} in the CLIP model. Our method applies to various model backbones and does not require any additional training or new parameters. Building upon SeTAR, we further demonstrate its effectiveness for fine-tuning initialization, referred to as SeTAR+FT.

We conduct extensive evaluations and achieve state-of-the-art performance on common OOD detection benchmarks for CLIP, including the ImageNet1K and Pascal-VOC benchmarks. Compared to vanilla MCM and GL-MCM, SeTAR with the CLIP backbone reduces FPR95 by 9.5% and 12.0% on average across two benchmarks, respectively. When further integrate fine-tuning into SeTAR, SeTAR+FT outperforms the state-of-the-art fine-tuning baselines LoCoOp (Miyai et al., 2023a) and LoRA (Hu et al., 2022). Moreover, we perform a comprehensive ablation study and analysis to verify and understand SeTAR. In summary, our key results and contributions:

1. We proposed SeTAR, a simple yet effective OOD detection method based on selective low-rank approximation. It is training-free as it only performs post-hoc modification to CLIP weight matrices. SeTAR applies to a variety of scoring functions and model backbones. It can be readily integrated with existing zero-shot OOD detection methods.
2. We further extend SeTAR to SeTAR+FT, which demonstrates the effectiveness of SeTAR in improving the performance of finetuning-based OOD detection methods and achieving new state-of-the-art results.
3. We extensively evaluate SeTAR and SeTAR+FT across a diverse set of OOD detection tasks. It consistently outperforms baseline methods and establishes new state-of-the-art results on CLIP-based OOD detection benchmarks. On ImageNet1K, SeTAR achieves an AUROC of 91.32% with CLIP backbone and GL-MCM score. The score further increases to 92.31% when combined with the finetuning-based detection method.
4. We perform comprehensive ablation studies and empirical analyses to verify and understand SeTAR. We hope that this work will shed light on future explorations on in-depth understanding of the SeTAR method.²

² Code are available at <https://github.com/X1A0X1A/SeTAR>.

2 Preliminaries

CLIP Architecture The CLIP model (Radford et al., 2021) contains an image encoder $E^v(\cdot)$ and a text encoder $E^t(\cdot)$, aligned by contrastive learning over web-scale image-text pairs. In this work, we focus on CLIP-ViT which has a vision Transformer (ViT) as the image encoder. Each ViT encoder layer consists of a multihead self-attention sublayer and a feed-forward sublayer (FFN). In the self-attention module, the hidden state is linearly projected into different spaces with learnable parameters W_q, W_k, W_v . The output of the multihead self-attention is concatenated and projected back with another trainable linear matrix W_o . In the feed-forward module, the hidden state is projected into a wider space with up-projection matrix W_{up} and then projected back using W_{down} after the non-linear activation function (Figure 1). Due to the similarity of the image and text encoder layers, we use the same notations for the linear matrices in these layers. Both encoders have a linear projector W_p on top to map from each encoder’s representation to a shared space for contrastive learning.

Zero-shot OOD Detection with CLIP Zero-shot OOD detection aims to separate ID and OOD data without an ID training dataset. Given the CLIP, the ID classes are defined by the classification task of interest, which differs from the classes used in CLIP pretraining. Accordingly, OOD is defined as classes not belonging to any ID class, making the OOD detector a binary classifier. MCM (Ming et al., 2022) and GL-MLM (Miyai et al., 2023b) are two zero-shot CLIP-based OOD detection methods. Formally, let \mathbf{x} be the test image and $\mathcal{T}_{in} = \{\mathbf{y}_c\}_{c=1}^K$ be the set of text prompts containing M ID class labels (e.g., "a photo of a [CLASS]"). The image is segmented into l image patches $\mathbf{x} = (x_1, \dots, x_l)$. Following CLIP, we add [cls] before the image patches and use the output of [cls] from the visual projector W_p as the global image feature ($h^v \in \mathbb{R}^d$). The outputs of other patches are projected by the visual projector as the local image features ($\mathbf{p}^v = (p_1^v, \dots, p_l^v) \in \mathbb{R}^{l \times d}$). For the text prompt $\mathbf{y}_c \in \mathcal{T}_{in}$, we add an additional [eos] after the text tokens and use the output feature of [eos] from the textual projector W_p as the concept feature of ID class c ($h_c^t \in \mathbb{R}^d$).

The label-wise image-concept matching (IWIC) score measures how the test image \mathbf{x} matches a concept \mathbf{y}_c and can be calculated using either global or local image features. The global IWIC score $s_c^G(\cdot)$ is defined as the cosine similarity between global image feature h^v and the concept feature h_c^t : $s_c^G(\mathbf{x}) = \cos_sim(h^v, h_c^t)$. The local IWIC score $s_c^L(\cdot)$ is the max-pooled cosine similarity of image patch features p_i^v and the concept feature h_c^t : $s_c^L(\mathbf{x}) = \max_i \cos_sim(p_i^v, h_c^t)$. The MCM and GL-MCM scores are then defined as:

$$S_{\text{MCM}}(\mathbf{x}) = \max_c \frac{e^{s_c^G(\mathbf{x})/\tau}}{\sum_{c=1}^K e^{s_c^G(\mathbf{x})/\tau}}, \quad (1)$$

$$S_{\text{GL-MCM}}(\mathbf{x}) = S_{\text{MCM}}(\mathbf{x}) + \max_c \frac{e^{s_c^L(\mathbf{x})/\tau'}}{\sum_{c=1}^K e^{s_c^L(\mathbf{x})/\tau'}}, \quad (2)$$

where τ and τ' are the temperature hyperparameters. MCM only uses global image feature, while GL-MCM additionally considers local image features. For ID data, both MCM and GL-MCM scores will be matched to one of the concept features with a high score; and vice versa. As a result, our OOD detection function can be formulated as:

$$G(\mathbf{x}) = \begin{cases} 1 & S(\mathbf{x}) \geq \lambda \\ 0 & S(\mathbf{x}) < \lambda \end{cases}, \quad (3)$$

where $S(\mathbf{x})$ is either the MCM or GL-MCM score, λ is the threshold value. By convention, $G(\mathbf{x}) = 1$ represents the ID class and $G(\mathbf{x}) = 0$ indicates the OOD class. The λ is chosen so that a high fraction of ID data (e.g., 95%) is above the threshold. We follow previous work (Miyai et al., 2023a) to use either MCM or GL-MCM score for OOD detection in this work.

3 Method

We introduce SeTAR, a training-free and effective technique for improving OOD detection performance (see Figure 1). Our key idea is to perform post-hoc modification to CLIP weight matrices by selectively replacing them with their low-rank approximations. It is complementary to existing CLIP-based zero-shot OOD detection methods and could be further extended to finetuning-based methods, which we term as SeTAR+FT.

3.1 OOD Detection with Selective Low-Rank Approximation

Low-Rank Approximation Given a linear matrix $W \in \mathbb{R}^{m \times n}$, its Singular Value Decomposition (SVD) is denoted as $W = U\Sigma V^\top$, where $U = [u_1, u_2, \dots, u_m] \in \mathbb{R}^{m \times m}$, $V = [v_1, v_2, \dots, v_n] \in \mathbb{R}^{n \times n}$, and $\Sigma \in \mathbb{R}^{m \times n}$ is a matrix whose entries are all zero except for the singular values of W . These singular values appear in decreasing order on the diagonal (i.e. $\sigma_i^\downarrow(W)$). The SVD of W can be reformulated as in Equation 4. Given a hyperparameter $r \in \mathbb{N}^+$, a rank- r approximation of W is matrix \widehat{W} that minimizes $\|W - \widehat{W}\|_2$ and satisfies $\text{rank}(\widehat{W}) \leq r$. The optimal solution of this problem \widehat{W} is provided by Eckart–Young–Mirsky theorem (Low-Rank Approximation, 2024) using Singular Value Decomposition (see Equation 5).

$$W = \sum_{i=1}^{\min(m,n)} \sigma_i^\downarrow(W) u_i v_i^\top, \quad (4)$$

$$\widehat{W} = \sum_{i=1}^r \sigma_i^\downarrow(W) u_i v_i^\top. \quad (5)$$

In this work, we will use the term **minor singular components** to refer to entries in the SVD corresponding to small singular values. These components are removed in low-rank approximation. The term of **principle singular components** is used to refer to entries in the SVD corresponding to large singular values. These components are kept in a low-rank approximation of the matrix.

OOD Detection with Selective Low-Rank Approximation Motivated by the effectiveness of SVD in capturing the most informative aspects of a matrix, we propose a method to enhance OOD detection. By decomposing a weight matrix W into its singular values and vectors, we can identify and retain the principle singular components that significantly contribute to the model’s performance. This approach ensures that the essential features of W are preserved while discarding the less critical minor singular components. Given a weight matrix W in CLIP (e.g., W_{up} or W_{k}), we replace the matrix with its low-rank approximation part \widehat{W} as described in Equation 5 (see Figure 1). Given the rank reduction ratio Θ , the rank of \widehat{W} is determined by $r(\widehat{W}) = \text{round}((1 - \Theta) \cdot r(W))$. This selective low-rank approximation leverages the compact representation provided by SVD to enhance the model’s ability to detect OOD instances effectively without requiring additional training. We demonstrate our method’s ability to improve OOD detection (Table 1) while maintaining ID classification performance (Table 7) in Section 4.2 and Section 4.5 .

HyperParameter Search Algorithm Due to the presence of many weight matrices in CLIP, each consisting of hundreds of singular values, conducting a complete search over all combinations of low-rank approximation weight matrices is impractical. Therefore, we propose a greedy search algorithm to determine the rank reduction ratio for each weight matrix. Among all linear weight matrices in each encoder layer, we focus on W_{up} as it is most effective according to our preliminary experiment. For simplicity, we assume both image and text encoders have N encoder layers. As shown in Algorithm 1, we search by first enumerating all N vision encoder layers sequentially from top to bottom and then all N text encoder layers in the same way. This search order is concisely denoted as searching from $2N$ to the first layer in CLIP. We compare different search algorithms in Section 4.4. The rank reduction ratio for each layer is the objective in SeTAR which is searched among the candidate list $\Theta = \{\Theta_0, \Theta_1, \dots, \Theta_J\}$ according to the loss on the validation set. We employ the LoCoOp loss (Equation 12) proposed in (Miyai et al., 2023a) as our loss function. This loss

Algorithm 1 The hyperparameter search in SeTAR.

Data: Valid set D .

Input: Layer length $2N$, rank reduction ratio candidates Θ with length J , loss \mathcal{L} on D WITHOUT SeTAR.

Result: Rank reduction ratio list \mathbf{T}^* with length $2N$.
 $\mathcal{L}^* = \mathcal{L}_0$; // Current best loss
for $\text{LayerNum } l \leftarrow 2N$ **to** 1 **do**

$\widehat{W}^* = W_{\text{up}}^l$ $T^*[l] = 0$ **for** counter $j \leftarrow 1$ **to** J **do**
 $r = \text{round}((1 - \Theta[j]) \cdot h)$

$\widehat{W} = \sum_{i=1}^r \sigma_i^\downarrow u_i v_i^\top$

Calculate loss \mathcal{L}_j^l on D by replacing W_{up}^l with

\widehat{W}

if $\mathcal{L}_j^l < \mathcal{L}^*$ **then**

$\widehat{W}^* = \widehat{W}$; $T^*[l] = \Theta[j]$; $\mathcal{L}^* = \mathcal{L}_j^l$;

end

end

$W_{\text{up}}^l := \widehat{W}^*$

end

return T^*

requires only ID images. It contains an ID loss for ID image classification and an OOD loss to push away pseudo OOD features from the ID class text embeddings where the pseudo OOD features are from ID-irrelevant nuisances (Equation 10) (e.g., backgrounds) in CLIP’s local features. We refer the readers to Miyai et al. (2023a) or Appendix B for more details. For $\Theta_j \in \Theta$, we remove Θ_j (in percent) singular values along with their corresponding singular vectors to obtain the approximated matrix \widehat{W}_{up} (Equation 5). It is worth noting that the rank reduction ratio candidate list includes $\Theta_0 = 0$, indicating that the weight matrix has the chance to remain unmodified.

With the searched rank reduction ratio, the weight matrix W_{up} in each CLIP layer is replaced and updated with its approximation. The SeTAR can be easily applied to different ViT backbones (Table 8), by replacing the model weight matrices with their low-rank approximations in a similar approach. Then SeTAR detects the OOD data samples following MCM (Equation 1), GL-MCM (Equation 2) or other scoring-based OOD detection method with the approximated model. We provide an example procedure of the greedy search in Listing 1 for better understanding.

3.2 OOD Detection with SeTAR-enhanced Low-rank Adaptation

SeTAR can be further combined with LoRA (Hu et al., 2022) as a novel low-rank adaptation method for OOD detection, which we refer to as **SeTAR+FT**. Specifically, we first apply SeTAR to the pre-trained CLIP model to obtain the reserved rank r for each weight matrix W . Then we have

$$W = \widehat{W} + B \times A \tag{6}$$

$$B = \sum_{i=r+1}^{\min(m,n)} \sqrt{\sigma_i^\downarrow(W)} u_i \tag{7}$$

$$A = \sum_{i=r+1}^{\min(m,n)} \sqrt{\sigma_i^\downarrow(W)} v_i^\top \tag{8}$$

where \widehat{W} is the low-rank approximation of W found by SeTAR, with A and B being the minor singular components. During finetuning, we keep \widehat{W} frozen and only update the low-rank matrix A and B . In this way, we retain the principle singular components in the original weight matrix and only update the minor singular components. Unlike LoRA, which evenly distributes the finetuning rank budget across all layers, SeTAR+FT adjusts the rank for each layer, resulting in more effective and efficient fine-tuning (Table 2 and Figure 6). More details are provided in Section 4.3.

4 Experiments

4.1 Experimental Setup

Dataset Following previous work (Ming et al., 2022; Miyai et al., 2023b), we use two real-world datasets created from ImageNet1K (Deng et al., 2009) and Pascal-VOC (Everingham et al., 2009) as the ID datasets. For OOD datasets, we follow Ming et al. (2022) to preprocess iNaturalist, SUN, Places and Texture, and follow Miyai et al. (2023b) to preprocess ImageNet22K and COCO data. For finetune experiments, we follow Miyai et al. (2023a) to use ImageNet1K as the ID dataset. The detailed description and statistics of the datasets are provided in Appendix C.

Settings Following existing studies (Ming et al., 2022; Miyai et al., 2023b,a), we use CLIP ViT-B/16³ (Radford et al., 2021) as our backbone. Both image and text encoders have 12 layers. More results with different backbones are in Section 4.4. The rank reduction ratio candidates range from 0 to 40% in 5% intervals. We use a temperature of 1⁴, unless stated otherwise. In all experiments, we use one CLIP text prompt: "a photo of a [CLASS],", where [CLASS] is the ID class name. We set hyperparameters λ (Equation 12) and top-K (Equation 10) according to the specific ID datasets and backbones. Detailed settings are in Table 10, with a sensitivity analysis in Section 4.4. For SeTAR+FT and LoRA experiments, the learning rate and epoch number are set to $1e-2$ and 5 for all

³<https://huggingface.co/openai/clip-vit-base-patch16>

⁴Temperature is set to 1.0 for the scaled CLIP logits, equivalent to the unscaled CLIP logits with a temperature of 100. We adopt the unscaled setting in our implementation.

Table 1: **Training-free results of FPR95(FPR) and AUROC(AUC) compared to zero-shot baselines on CLIP-base.** Bold values represent the highest performance. † is cited from Miyai et al. (2023b), where \diamond represents the absence of reporting in the paper. * denotes the result of our re-run. – denotes the OOD dataset has overlapping categories with the ID dataset. We do not report standard deviations since no training is involved.

Method	iNaturalist		SUN		Places		Texture		ImageNet22K		COCO		Average	
	FPR↓	AUC↑	FPR↓	AUC↑	FPR↓	AUC↑	FPR↓	AUC↑	FPR↓	AUC↑	FPR↓	AUC↑	FPR↓	AUC↑
ImageNet1K														
MCM Score														
Vanilla MCM†	30.91	94.61	37.59	92.57	44.69	89.77	57.77	86.11	-	-	-	-	42.74	90.77
Vanilla MCM*	32.07	94.43	38.65	92.37	43.73	90.03	57.89	86.13	-	-	-	-	43.09	90.74
SeTAR	26.92	94.67	35.57	92.79	42.64	90.16	55.83	86.58	-	-	-	-	40.24	91.05
GL-MCM Score														
Vanilla GL-MCM†	15.18	96.71	30.42	93.09	38.85	89.90	57.93	83.63	-	-	-	-	35.47	90.83
Vanilla GL-MCM*	15.34	96.62	30.65	93.01	37.76	90.07	57.41	83.73	-	-	-	-	35.29	90.86
SeTAR	13.36	96.92	28.17	93.36	36.80	90.40	54.17	84.59	-	-	-	-	33.12	91.32
Pascal-VOC														
MCM Score														
Vanilla MCM†	8.20	98.23	28.60	94.68	\diamond	\diamond	51.70	91.45	51.40	90.94	54.50	89.02	38.88	92.86
Vanilla MCM*	7.24	98.23	27.91	94.56	32.40	92.45	51.61	91.89	50.60	91.42	53.70	89.30	37.24	92.98
SeTAR	4.59	98.71	24.91	95.15	28.46	93.21	40.44	93.58	48.25	92.08	48.10	89.70	32.46	93.74
GL-MCM Score														
Vanilla GL-MCM†	4.20	98.71	23.10	94.66	\diamond	\diamond	43.00	92.84	41.00	92.38	44.30	90.48	31.12	93.81
Vanilla GL-MCM*	4.33	98.81	22.94	94.63	26.20	93.11	41.61	92.88	37.88	93.17	43.70	90.71	29.44	93.88
SeTAR	3.66	98.96	21.93	94.81	25.04	93.62	20.35	96.36	31.47	94.31	40.70	91.19	23.86	94.87

experiments. The LoRA rank r is set to match the trainable parameters of SeTAR+FT. Detailed settings are in Table 11. We report results from three runs with seeds 3, 4, 5⁵. All experiments are conducted on a single NVIDIA RTX 4090 GPU. The time cost for low-rank approximation with CLIP-base on the ImageNet1K validation set is about 20 minutes.

Metrics We use the following metrics for evaluation. (1) the false positive rate (FPR95) for out-of-distribution (OOD) samples at a fixed true positive rate (TPR) of 95% for in-distribution samples, with lower values targeting better performance; and (2) the area under the receiver operating characteristic curve (AUROC) for OOD samples, with higher values indicating better performance.

Baselines We evaluate SeTAR against MCM (Ming et al., 2022) and GL-MCM (Miyai et al., 2023b), state-of-the-art zero-shot OOD detection methods on CLIP. We also compare SeTAR+FT with fine-tuning baselines NPOS (Tao et al., 2023), CoOp (Zhou et al., 2022), LoCoOp (Miyai et al., 2023a), and LoRA (Hu et al., 2022). More details are in Appendix D.

4.2 Training-free Results

The training-free OOD detection performances are summarized in Table 1. Compared with zero-shot baselines, a salient observation is that on both MCM and GL-MCM, using SeTAR outperforms the vanilla method by a large margin across all OOD detection tasks. For example, using Pascal-VOC as ID, SeTAR yields an average reduction of 12.84% FPR95 on MCM and 18.95% FPR95 on GL-MCM. Considering that SeTAR is generally applicable and training-free, these results are very encouraging. Comparing SeTAR with scoring function MCM and GL-MCM, SeTAR+GL-MCM performs better on all OOD detection tasks. However, the superiority of GL-MCM score over MCM appears to be contingent upon the choice of the model backbone. As evidenced in Table 8, SeTAR+MCM demonstrates superior performance with an average FPR95 reduction of 8.30% compared to SeTAR+GL-MCM with CLIP-large as the backbone on ImageNet1K.

4.3 Fine-tuning Results

In this section, we compare SeTAR+FT with fine-tuning baselines, including NPOS (Tao et al., 2023), CoOp (Zhou et al., 2022), LoCoOp (Miyai et al., 2023a) and LoRA (Hu et al., 2022). LoCoOp is the state-of-the-art prompt-learning OOD detection method on CLIP. LoRA is a representative parameter-efficient fine-tuning method. Following previous work (Tao et al., 2023; Zhou et al., 2022; Miyai et al., 2023a), we report the results on the ImageNet1K benchmark in Table 2. We observe that SeTAR+FT outperforms all baselines on both MCM and GL-MCM scoring functions. For example, with CLIP-base as the backbone, SeTAR+FT achieves an average FPR95 reduction of 3.97% and 6.67% compared to LoCoOp and LoRA.

⁵For SeTAR, the results are the same under different random seeds as it does not require training.

Moreover, when scaled up to CLIP-large, SeTAR+FT outperforms LoCoOp and LoRA by 17.92% and 12.45% FPR95 on the same benchmark. Similar results are observed on Swin Transformer (Liu et al., 2021), where SeTAR+FT outperforms LoRA by 17.36% FPR95 on the MSP scoring function and 36.80% FPR95 on the Energy scoring function. These results demonstrate the effectiveness and scalability of SeTAR+FT in improving the OOD detection performance of CLIP.

Furthermore, we found that SeTAR+FT is more effective than LoRA, as demonstrated in Figure 6. The results show that SeTAR+FT achieves a quicker convergence and lower loss than LoRA during the fine-tuning process, especially OOD loss, indicating that SeTAR+FT is more effective in adapting the pre-trained weights to the OOD detection task.

4.4 Ablation Study

In this section, we conduct ablation studies with CLIP-base to understand our design choices.

Image v.s. Text modality Table 3 shows an ablation study on the modality involved in SeTAR. As shown, the vision modality outperforms the text modality. When considering the vision modality alone and the combined vision+text modality, the latter either outperforms or achieves comparable average results to the former. Consequently, we make modifications to both the vision and text modalities in SeTAR to enhance overall performance.

Different weight types In this part, we present empirical evidence for modifying W_{up} . We first compare the performance of SeTAR with different types of weight matrix in each Transformer layer, including W_q , W_k , W_v , W_o , W_{up} and W_{down} . As shown in Figure 2 and Figure 3 of Appendix F, the X -axis denotes the number of weight matrixes (layers) that we have searched, while the Y -axis is the average AUROC and FPR95. The results show that W_{up} consistently outperforms other weight matrices in terms of both AUROC and FPR95. In addition to weight matrices in each transformer layer, CLIP has one projection matrix W_p on top of each encoder, which serves to project image/text representations into a shared space. In Table 4, we compare the performance of SeTAR with and without modifying W_p . We search W_p first right before searching the image/text encoder. The results show that frozen W_p brings a reduction of 4.20% FPR95. Consequently, we keep W_p frozen in SeTAR.

Different Search Algorithms At each step of the greedy search, SeTAR traverses the subsequent W_{up} in a predefined order and searches over different thresholds. We compare our method with two alternatives: modality-interleaved greedy search (MIS) and layer-exhaustive search (LES). MIS searches the image and text layers in an interleaved manner, while LES simultaneously searches over both layers and thresholds at each step. SeTAR-S, has linear complexity with respect to the number of model layers, similar to MIS, whereas LES has quadratic complexity.

Table 2: **Fine-tuning results on ImageNet1K benchmark.** Bold values indicate the highest performance. † is cited from Tao et al. (2023). * denotes our re-run results, \pm indicates the standard deviation from 3 runs.

CLIP-base	MCM Score		GL-MCM Score	
	FPR95↓	AUROC↑	FPR95↓	AUROC↑
NPOS†	42.20	90.43	36.86	90.37
CoOp†	44.81	90.03	36.58	90.25
LoCoOp†	40.17	91.53	33.52	92.14
LoCoOp*	39.76 \pm 4.06	91.22 \pm 0.52	34.14 \pm 1.64	91.73 \pm 0.17
LoRA*	41.67 \pm 0.14	90.85 \pm 0.01	34.36 \pm 0.11	90.88 \pm 0.01
SeTAR+FT	38.77\pm0.22	91.55\pm0.01	32.19\pm0.20	92.31\pm0.05

CLIP-large	MCM Score		GL-MCM Score	
	FPR95↓	AUROC↑	FPR95↓	AUROC↑
LoCoOp*	40.74 \pm 3.80	91.13 \pm 0.79	46.74 \pm 4.19	89.32 \pm 0.80
LoRA*	38.62 \pm 0.07	91.66 \pm 0.02	43.39 \pm 0.01	89.76 \pm 0.03
SeTAR+FT	34.75\pm0.55	92.86\pm0.15	37.05\pm0.59	91.83\pm0.12

Swin-base	MSP Score		Energy Score	
	FPR95↓	AUROC↑	FPR95↓	AUROC↑
LoRA*	57.02 \pm 0.03	80.49 \pm 0.01	62.17 \pm 0.02	72.80 \pm 0.00
SeTAR+FT	47.12\pm0.42	87.80\pm0.44	39.29\pm0.57	88.01\pm0.51

Table 3: **Ablation study on modality.**

Score	Vision		Text		Vision+Text	
	FPR↓	AUC↑	FPR↓	AUC↑	FPR↓	AUC↑
ImageNet1K						
MCM	40.27	91.24	42.78	90.50	40.24	91.05
GL-MCM	32.97	91.60	35.82	90.55	33.12	91.32
Pascal-VOC						
MCM	33.19	93.45	33.47	93.42	32.46	93.74
GL-MCM	24.88	94.51	24.59	94.52	23.86	94.87

Table 4: **Comparison results of SeTAR with and without considering projection matrix W_p .**

Score	Vanilla		SeTAR w W_p		SeTAR w/o W_p	
	FPR↓	AUC↑	FPR↓	AUC↑	FPR↓	AUC↑
ImageNet1K						
MCM	43.09	90.74	41.79	90.74	40.24	91.05
GL-MCM	35.29	90.86	34.30	91.24	33.12	91.32
Pascal-VOC						
MCM	37.24	92.98	35.94	93.32	32.46	93.74
GL-MCM	29.44	93.88	23.34	94.82	23.86	94.87

Table 5 presents the comparison results. SeTAR-S demonstrates better overall performance than MIS. Notably, MIS fails when the image and text towers have different layer counts (e.g., CLIP-large with 24 image layers and 12 text layers). Therefore, we choose SeTAR-S for better generalization. Compared to LES, SeTAR-S performs better in terms of both FPR95 and AUROC, as LES’s locally optimal algorithm may not achieve a global optimal solution. These results validate the superiority of our top-to-bottom layer search strategy.

Table 5: **Results for different search algorithms.** Here LES, MIS and SeTAR-S stand for layer-exhaustive search, modality-interleave greedy search, and the search algorithm of SeTAR.

Score	LES		MIS		SeTAR-S	
	FPR↓	AUC↑	FPR↓	AUC↑	FPR↓	AUC↑
ImageNet1K						
MCM	41.99	90.78	40.55	91.00	40.24	91.05
GL-MCM	33.90	91.08	33.36	91.29	33.12	91.32
Pascal-VOC						
MCM	35.11	93.60	33.93	93.58	32.46	93.74
GL-MCM	24.48	94.57	22.87	94.84	23.86	94.87

Different Prune Strategies Inspired from SVD, SeTAR modified the model weights by pruning the minor singular components, and retains the principle components that contribute the most to the model’s performance. To validate this design, we compare SeTAR with two alternatives: principal component pruning and random pruning. Principal component pruning takes an opposite approach, retaining minor components and pruning major ones. Random pruning, on the other hand, prunes weights randomly. As shown in Table 6, principle pruning suffers from a significant performance drop compared to SeTAR, while random pruning performs slightly better than principle pruning. These results demonstrate the effectiveness of SeTAR’s design choice in pruning the minor components.

Table 6: **Results for different pruning strategies.**

Score	Principle		Random		Minor	
	FPR↓	AUC↑	FPR↓	AUC↑	FPR↓	AUC↑
ImageNet1K						
MCM	43.09	90.74	43.09	90.74	40.24	91.05
GL-MCM	35.29	90.86	35.29	90.86	33.12	91.32
Pascal-VOC						
MCM	38.20	92.44	33.57	93.09	32.46	93.74
GL-MCM	25.36	93.67	26.20	94.66	23.86	94.87

Sensitivity Analysis on λ and top-K In this section, we present the sensitivity analysis of the hyperparameters λ (Figure 4) and top-K (Figure 5). As observed in Figure 4, the average AUROC remains stable at lower values and slightly decreases as λ increases for both SeTAR+MCM and SeTAR+GL-MCM. Notably, the optimal setting of λ may vary depending on the model backbone, with our experiments indicating that CLIP-large may require a larger λ than CLIP-base. Regarding top-K, which controls the number of OOD regions considered, higher top-K values include more OOD regions. When top-K equals the number of ID classes, the model considers all OOD regions. Conversely, when top-K is set to 0, the model focuses solely on ID loss. Figure 5 demonstrates the impact of varying top-K on AUROC and FPR95. SeTAR exhibits high robustness to changes in top-K, except at extreme values such as 0 or the maximum number of ID classes.

4.5 Analyses

Can SeTAR improve image classification?

To evaluate the impact of SeTAR and SeTAR+FT on classification accuracy, we present our results on ID dataset ImageNet1K and OOD datasets SUN, Places and Texture in Table 7⁶. SeTAR effectively maintains the average accuracy, with minor variations observed across different datasets. Among the fine-tuned baselines, LoCoOp exhibits a 1% decrease in accuracy compared to Vanilla CLIP, whereas LoRA shows an improvement of 0.94%. Notably, SeTAR+FT surpasses both baselines, improving the average accuracy by 1.45% compared to Vanilla CLIP. These results highlight the efficacy of SeTAR and SeTAR+FT in improving OOD detection without compromising classification accuracy.

Table 7: **Image classification results with different methods.** We use ImageNet1K (IN1K) as ID dataset. * denotes the results of our re-run. The results are averaged over 3 runs.

Method	IN1K	SUN	Places	Texture	Average
Vanilla CLIP*	64.07	75.77	45.65	43.60	57.27
LoCoOp*	64.93	75.89	46.47	37.79	56.27
LoRA*	65.43	76.86	46.58	43.98	58.21
SeTAR	63.97	75.50	45.81	43.76	57.26
SeTAR+FT	67.02	77.94	46.64	43.28	58.72

SeTAR is effective on different model backbones. To examine the effectiveness of SeTAR on different model backbones, we compare OOD detection performance with CLIP-large (CLIP

⁶We do not report classification accuracy on iNaturalist as we failed to match the labels for the OOD test set.

ViT-L/14⁷) and Swin Transformer (Swin-V2-B/16@256px-ImageNet1K⁸) (Liu et al., 2021) in addition to CLIP-base. The Swin Transformer (Liu et al., 2022) is a novel unimodal model trained with the ImageNet1K classification dataset. We apply SeTAR to the image ViT as it lacks a text encoder. We follow common practice and consider two scoring functions for Swin Transformer: MSP (Hendrycks & Gimpel, 2017), using the softmax confidence score to detect OOD samples, and the Energy score (Liu et al., 2020), utilizing information in logits for OOD detection. We set the temperature $T = 0.1$ for the Energy score. As shown in Table 8, SeTAR outperforms baselines across all model backbones and scoring functions. Notably, applying SeTAR to Swin Transformer with the Energy score significantly reduces FPR95 by 20.61% on average. These results highlight SeTAR’s potential for improving OOD detection with unimodal image encoders. Our results on SeTAR+FT (Table 2) further confirm its effectiveness across different model backbones.

Table 8: **Results for different model backbones.**

Backbone	Score	Vanilla Method		SeTAR	
		FPR↓	AUC↑	FPR↓	AUC↑
ImageNet1K					
CLIP-large	MCM	37.19	91.73	36.26	91.92
CLIP-large	GL-MCM	40.65	89.98	39.54	90.22
Swin-base	MSP	59.25	84.12	56.05	85.77
Swin-base	Energy	65.01	76.10	51.61	84.42
Pascal-VOC					
CLIP-large	MCM	52.21	91.68	42.57	92.91
CLIP-large	GL-MCM	43.96	92.45	31.12	94.00

5 Related Work

Out-of-distribution detection Previous work explores OOD detection with unimodal (DeVries & Taylor, 2018; Hendrycks & Gimpel, 2017; Hu & Khan, 2021; Zheng et al., 2020; Zhou et al., 2021) and multimodal (Fort et al., 2021; Ming et al., 2022; Tao et al., 2023; Miyai et al., 2023a) models. Numerous methodologies (Lee et al., 2018; Huang et al., 2021; Sun et al., 2022; Wang et al., 2022; Wu et al., 2023) have been developed to tackle OOD detection in computer vision. Existing CLIP-based OOD detection methods include zero-shot (Fort et al., 2021; Ming et al., 2022; Miyai et al., 2023b; Dai et al., 2023; Wang et al., 2023) and fine-tuning (Ming & Li, 2023; Tao et al., 2023; Miyai et al., 2023a). Zero-shot methods like MCM (Ming et al., 2022) and GL-MCM (Miyai et al., 2023b) don’t require in-distribution training data but may perform suboptimally due to domain gaps. Fine-tuning methods (Ming & Li, 2023; Tao et al., 2023; Miyai et al., 2023a) improve OOD detection by adapting to in-distribution data but risk damaging the pretraining representations, needing careful training strategies. Our proposed SeTAR complements various scoring functions and model backbones for OOD detection.

Low-rank approximations of weight matrices Neural networks trained with over-parameterization often exhibit low-rank properties (Oymak et al., 2019). These properties are utilized in both model training (Povey et al., 2018; Hu et al., 2022) and post-hoc processing (Hajimolahoseini et al., 2021; Sharma et al., 2023). In training, some works (Sainath et al., 2013; Zhang et al., 2014; Zhao et al., 2016) impose low-rank constraints, while LoRA (Hu et al., 2022) adapts pretrained LLMs to downstream tasks using trainable low-rank matrices. For post-hoc processing, pruning methods (Yu et al., 2017; Hajimolahoseini et al., 2021) reduce weight matrix ranks by retaining top-K components from SVD. While pruning preserves model behavior, performance declines with increased intervention. Unlike these approaches, our work employs a selective rank reduction strategy.

6 Conclusion

We propose SeTAR, a simple and effective OOD detection method using post-hoc low-rank approximation on weight matrices W_{up} with a top-down, image-to-text greedy search. SeTAR offers several advantages: (1) training-free, (2) scalable to unimodal and multimodal models, and (3) complementary to existing OOD scoring functions. Building on SeTAR, we introduce SeTAR-FT, a finetuning method that adapts the model to in-distribution data for improved OOD detection. We evaluate SeTAR and SeTAR-FT on large-scale benchmarks, including ImageNet1K and Pascal-VOC. Results show that both achieve state-of-the-art OOD detection performance. We hope our work inspires further research and contributes to more robust and reliable models.

⁷<https://huggingface.co/openai/clip-vit-large-patch14>

⁸<https://huggingface.co/microsoft/swinv2-base-patch4-window16-256>

References

- Bai, H., Canal, G., Du, X., Kwon, J., Nowak, R. D., and Li, Y. Feed two birds with one scone: Exploiting wild data for both out-of-distribution generalization and detection. In *International Conference on Machine Learning*, 2023.
- Caesar, H., Uijlings, J., and Ferrari, V. Coco-stuff: Thing and stuff classes in context. In *CVPR*, 2018.
- Cimpoi, M., Maji, S., Kokkinos, I., Mohamed, S., and Vedaldi, A. Describing textures in the wild. In *CVPR*, 2014.
- Dai, Y., Lang, H., Zeng, K., Huang, F., and Li, Y. Exploring large language models for multi-modal out-of-distribution detection. *ArXiv*, abs/2310.08027, 2023. URL <https://api.semanticscholar.org/CorpusID:263909127>.
- Deng, J., Dong, W., Socher, R., Li, L.-J., Li, K., and Fei-Fei, L. Imagenet: A large-scale hierarchical image database. In *CVPR*, 2009.
- DeVries, T. and Taylor, G. W. Learning confidence for out-of-distribution detection in neural networks. *arXiv preprint:1802.04865*, 2018.
- Emmott, A., Das, S., Dietterich, T., Fern, A., and Wong, W.-K. A meta-analysis of the anomaly detection problem. *arXiv preprint:1503.01158*, 2016.
- Everingham, M., Van Gool, L., Williams, C. K., Winn, J., and Zisserman, A. The pascal visual object classes (voc) challenge. *IJCV*, 88:303–308, 2009.
- Fort, S., Ren, J., and Lakshminarayanan, B. Exploring the limits of out-of-distribution detection. In *NeurIPS*, 2021.
- Hajimolahoseini, H., Rezagholizadeh, M., Partovinia, V., Tahaei, M. S., Awad, O. M., and Liu, Y. Compressing pre-trained language models using progressive low rank decomposition. In *NeurIPS*, 2021.
- Hendrycks, D. and Gimpel, K. A baseline for detecting misclassified and out-of-distribution examples in neural networks. In *ICLR*, 2017.
- Hendrycks, D., Liu, X., Wallace, E., Dziedzic, A., Krishnan, R., and Song, D. Pretrained transformers improve out-of-distribution robustness. In *Proceedings of the 58th Annual Meeting of the Association for Computational Linguistics*, pp. 2744–2751, Online, July 2020.
- Hendrycks, D., Basart, S., Mazeika, M., Mostajabi, M., Steinhardt, J., and Song, D. Scaling out-of-distribution detection for real-world settings. In *ICML*, 2022.
- Hu, E. J., yelong shen, Wallis, P., Allen-Zhu, Z., Li, Y., Wang, S., Wang, L., and Chen, W. LoRA: Low-rank adaptation of large language models. In *ICLR*, 2022.
- Hu, Y. and Khan, L. Uncertainty-aware reliable text classification. In *Proceedings of the 27th ACM SIGKDD Conference on Knowledge Discovery & Data Mining*, pp. 628–636, New York, NY, USA, 2021.
- Huang, R., Geng, A., and Li, Y. On the importance of gradients for detecting distributional shifts in the wild. In *NeurIPS*, 2021.
- Lee, K., Lee, K., Lee, H., and Shin, J. A simple unified framework for detecting out-of-distribution samples and adversarial attacks. In *NeurIPS*, 2018.
- Li, J., Li, D., Savarese, S., and Hoi, S. BLIP-2: bootstrapping language-image pre-training with frozen image encoders and large language models. In *Proceedings of the 40th International Conference on Machine Learning*, 2023.
- Liang, S., Li, Y., and Srikant, R. Enhancing the reliability of out-of-distribution image detection in neural networks. In *ICLR*, 2018.
- Lin, T.-Y., Maire, M., Belongie, S., Hays, J., Perona, P., Ramanan, D., Dollár, P., and Zitnick, C. L. Microsoft coco: Common objects in context. In *ECCV*, 2014.

- Liu, W., Wang, X., Owens, J., and Li, Y. Energy-based out-of-distribution detection. In *NeurIPS*, 2020.
- Liu, Z., Lin, Y., Cao, Y., Hu, H., Wei, Y., Zhang, Z., Lin, S., and Guo, B. Swin transformer: Hierarchical vision transformer using shifted windows. In *ICCV*, 2021.
- Liu, Z., Hu, H., Lin, Y., Yao, Z., Xie, Z., Wei, Y., Ning, J., Cao, Y., Zhang, Z., Dong, L., Wei, F., and Guo, B. Swin transformer v2: Scaling up capacity and resolution, 2022.
- Low-Rank Approximation. Low-rank approximation — Wikipedia, the free encyclopedia, January 2024. https://en.wikipedia.org/w/index.php?title=Low-rank_approximation&oldid=1196167027.
- Ming, Y. and Li, Y. How does fine-tuning impact out-of-distribution detection for vision-language models? *International Journal of Computer Vision*, 132(2):596–609, September 2023. ISSN 1573-1405. doi: 10.1007/s11263-023-01895-7. URL <http://dx.doi.org/10.1007/s11263-023-01895-7>.
- Ming, Y., Cai, Z., Gu, J., Sun, Y., Li, W., and Li, Y. Delving into out-of-distribution detection with vision-language representations. In *NeurIPS*, 2022.
- Miyai, A., Yu, Q., Irie, G., and Aizawa, K. Locoop: Few-shot out-of-distribution detection via prompt learning. In *Thirty-Seventh Conference on Neural Information Processing Systems*, 2023a.
- Miyai, A., Yu, Q., Irie, G., and Aizawa, K. Zero-shot in-distribution detection in multi-object settings using vision-language foundation models. *arXiv preprint arXiv:2304.04521*, 2023b.
- Oymak, S., Fabian, Z., Li, M., and Soltanolkotabi, M. Generalization guarantees for neural networks via harnessing the low-rank structure of the jacobian, 2019.
- Povey, D., Cheng, G., Wang, Y., Li, K., Xu, H., Yarmohammadi, M. A., and Khudanpur, S. Semi-orthogonal low-rank matrix factorization for deep neural networks. In *Interspeech*, 2018. URL <https://api.semanticscholar.org/CorpusID:4949673>.
- Radford, A., Kim, J. W., Hallacy, C., Ramesh, A., Goh, G., Agarwal, S., Sastry, G., Askell, A., Mishkin, P., Clark, J., et al. Learning transferable visual models from natural language supervision. In *ICML*, 2021.
- Russakovsky, O., Deng, J., Su, H., Krause, J., Satheesh, S., Ma, S., Huang, Z., Karpathy, A., Khosla, A., Bernstein, M., et al. Imagenet large scale visual recognition challenge. *IJCV*, 115(3):211–252, 2015.
- Sainath, T. N., Kingsbury, B., Sindhvani, V., Arisoy, E., and Ramabhadran, B. Low-rank matrix factorization for deep neural network training with high-dimensional output targets. In *2013 IEEE international conference on acoustics, speech and signal processing*, pp. 6655–6659. IEEE, 2013.
- Sharma, P., Ash, J. T., and Misra, D. The truth is in there: Improving reasoning in language models with layer-selective rank reduction, 2023.
- Sun, Y., Ming, Y., Zhu, X., and Li, Y. Out-of-distribution detection with deep nearest neighbors. In *ICML*, 2022.
- Tan, M., Yu, Y., Wang, H., Wang, D., Potdar, S., Chang, S., and Yu, M. Out-of-domain detection for low-resource text classification tasks. In *Proceedings of the 2019 Conference on Empirical Methods in Natural Language Processing and the 9th International Joint Conference on Natural Language Processing (EMNLP-IJCNLP)*, pp. 3566–3572, Hong Kong, China, November 2019.
- Tao, L., Du, X., Zhu, X., and Li, Y. Non-parametric outlier synthesis. In *ICLR*, 2023.
- Van Horn, G., Mac Aodha, O., Song, Y., Cui, Y., Sun, C., Shepard, A., Adam, H., Perona, P., and Belongie, S. The inaturalist species classification and detection dataset. In *CVPR*, 2018.
- Wang, H., Liu, W., Bocchieri, A., and Li, Y. Can multi-label classification networks know what they don’t know? In *NeurIPS*, 2021.

- Wang, H., Li, Z., Feng, L., and Zhang, W. Vim: Out-of-distribution with virtual-logit matching. In *CVPR*, 2022.
- Wang, H., Li, Y., Yao, H., and Li, X. Clipn for zero-shot ood detection: Teaching clip to say no. *2023 IEEE/CVF International Conference on Computer Vision (ICCV)*, pp. 1802–1812, 2023. URL <https://api.semanticscholar.org/CorpusID:261076240>.
- Wu, Q., Chen, Y., Yang, C., and Yan, J. Energy-based out-of-distribution detection for graph neural networks. *ArXiv*, abs/2302.02914, 2023. URL <https://api.semanticscholar.org/CorpusID:256615740>.
- Xiao, J., Hays, J., Ehinger, K. A., Oliva, A., and Torralba, A. Sun database: Large-scale scene recognition from abbey to zoo. In *CVPR*, 2010.
- Xu, K., Ren, T., Zhang, S., Feng, Y., and Xiong, C. Unsupervised out-of-domain detection via pre-trained transformers. In *ACL*, 2021.
- Yu, J., Wang, Z., Vasudevan, V., Yeung, L., Seyedhosseini, M., and Wu, Y. CoCa: Contrastive captioners are image-text foundation models. *arXiv preprint arXiv:2205.01917*, 2022.
- Yu, X., Liu, T., Wang, X., and Tao, D. On compressing deep models by low rank and sparse decomposition. *2017 IEEE Conference on Computer Vision and Pattern Recognition (CVPR)*, pp. 67–76, 2017. URL <https://api.semanticscholar.org/CorpusID:24553488>.
- Zhang, Y., Chuangsuwanich, E., and Glass, J. R. Extracting deep neural network bottleneck features using low-rank matrix factorization. *2014 IEEE International Conference on Acoustics, Speech and Signal Processing (ICASSP)*, pp. 185–189, 2014. URL <https://api.semanticscholar.org/CorpusID:1791734>.
- Zhao, Y., Li, J., and Gong, Y. Low-rank plus diagonal adaptation for deep neural networks. *2016 IEEE International Conference on Acoustics, Speech and Signal Processing (ICASSP)*, pp. 5005–5009, 2016. URL <https://api.semanticscholar.org/CorpusID:10506309>.
- Zheng, Y., Chen, G., and Huang, M. Out-of-domain detection for natural language understanding in dialog systems. *IEEE/ACM Transactions on Audio, Speech, and Language Processing*, 28: 1198–1209, 2020.
- Zhou, B., Lapedriza, A., Khosla, A., Oliva, A., and Torralba, A. Places: A 10 million image database for scene recognition. *TPAMI*, 40(6):1452–1464, 2017.
- Zhou, K., Yang, J., Loy, C. C., and Liu, Z. Learning to prompt for vision-language models. *IJCV*, 2022.
- Zhou, W., Liu, F., and Chen, M. Contrastive out-of-distribution detection for pretrained transformers. In *Proceedings of the 2021 Conference on Empirical Methods in Natural Language Processing*, pp. 1100–1111, Online and Punta Cana, Dominican Republic, November 2021.

A Impact Statements

Limitation While we demonstrate the effectiveness of our method on OOD detection, we acknowledge that our work has several limitations. First, despite we show the robustness of our method to hyperparameters, the optimal hyperparameters may vary across different model backbones. Future work is needed to explore the autonomous selection of hyperparameters. Second, we design SeTAR+FT in a simple and straightforward manner, which may not be the most efficient or effective way to adapt the model to the ID downstream data. More sophisticated strategies for model adaptation are worth exploring in future research. Third, we only conduct experiments to detect visual OOD inputs and ignore inputs in other modalities such as textual, audio and video. This is primarily because our model is based on CLIP. Exploring the development of OOD detectors across diverse modalities remains an active research topic for future investigation.

Ethical Considerations Our study addresses the challenge of OOD detection through low-rank approximation, which is particularly relevant for ensuring the reliability and trustworthiness of vision-and-language pre-trained models. Future investigations on fairness, privacy and transparency neural-based models should be encouraged to mitigate the existing data biases and safety problems for a responsible, helpful and trustworthy AI system in diverse real-world applications.

Future Societal Consequences Our proposed SeTAR achieves impressive OOD detection performance, which is beneficial to various real-world machine learning applications, such as healthcare and autonomous vehicles. The identification of anomalies or unexpected data points is crucial for decision-making and risk management with AI models. A better OOD detector facilitates the development of trustworthy machine-learning models that can reject unknown data inputs and help alleviate the hallucination problem. Moreover, better OOD detectors like SeTAR can help to select and label the unfamiliar data samples to further train a stronger model in the wild.

B Loss Function

To improve the model’s OOD detection ability, it is crucial to define a loss function that pushes OOD samples far from ID samples while keeping ID samples close to each other. However, since OOD samples are unavailable during development, we address this issue by using the LoCoOp loss (Miyai et al., 2023a) for both SeTAR and SeTAR+FT. The main idea is to create pseudo OOD features with ID-irrelevant nuisances (e.g., backgrounds) in CLIP’s local features.

Specifically, we divide the image into patches, represented by the set of all patch indices $I = \{0, 1, 2, \dots, H \times W - 1\}$, where H and W denote the height and width of the patch features. Next, we compute the cosine similarity between the image patch features p_i^v and the text features h_c^t of the image label. The classification prediction probabilities for each patch i are then given by:

$$p_i(y = m|\mathbf{x}) = \frac{\exp(\cos_sim(p_i^v, h_c^t)/\tau')}{\sum_{c=1}^K \exp(\cos_sim(p_i^v, h_c^t)/\tau')} \quad (9)$$

For a given image patch related to an ID category, the corresponding ID label should be among its top-K predictions. Conversely, for patches unrelated to the ID label, such as background regions, the ID label should be excluded from the top-K predictions. Based on this intuition, the indices of ID-irrelevant regions within an image are defined by Equation 10, where $\text{rank}(p_i(y = \mathbf{y}|\mathbf{x}))$ denotes the rank of the true class \mathbf{y} among all ID classes, and K is the hyperparameter.

$$J = \{i \mid \text{rank}(p_i(y = \mathbf{y}|\mathbf{x})) > K\} \quad (10)$$

After identifying out-of-distribution (OOD) regions, it is expected that their image features will differ significantly from the ID text embeddings. To enhance this distinction, entropy maximization is employed to increase the entropy of $p_j(y|\mathbf{x})$, where p_j denotes the classification prediction probabilities for region $j \in J$. The entropy maximization is formally defined as follows:

$$\mathcal{L}_{\text{ood}} = -H(p_j) \quad (11)$$

Here, $H(\cdot)$ represents the entropy function. The overall loss function combines the ID loss (cross-entropy loss for ID predictions) with the OOD loss. Here λ is the hyperparameter that regulates the proportion of the OOD loss.

$$\mathcal{L} = \mathcal{L}_{\text{id}} + \lambda \mathcal{L}_{\text{ood}} \quad (12)$$

C Data

Table 9: **The statistics of the dataset used in this paper.** ‘ID’ and ‘OOD’ denote in-distribution and out-of-distribution, respectively.

Data	Type	Valid Size	Test Size
ImageNet1K (Deng et al., 2009)	ID	1,000	50,000
Pascal-VOC (Everingham et al., 2009)	ID	94	906
iNaturalist (Van Horn et al., 2018)	OOD	0	10,000
SUN (Xiao et al., 2010)	OOD	0	10,000
Places (Zhou et al., 2017)	OOD	0	10,000
Texture (Cimpoi et al., 2014)	OOD	0	5,640
ImageNet22K (Russakovsky et al., 2015)	OOD	0	18,335
COCO (Lin et al., 2014)	OOD	0	1,000

We use two real-world datasets created from ImageNet1K (Deng et al., 2009) and Pascal-VOC (Everingham et al., 2009) as the ID dataset. We use ImageNet-1K validation set as the ID test set following Ming et al. (2022), and preprocess Pascal-VOC following Miyai et al. (2023b). We build two ID validation sets for low-rank approximation. The ID validation set of ImageNet1K is collected by sampling one image for each label from the ImageNet1K training set. For Pascal-VOC, For Pascal-VOC, We randomly sample 10% images as the ID validation set and leave the rest as the ID test set.

For OOD datasets, we follow Ming et al. (2022) to preprocess iNaturalist, SUN, Places and Texture, and follow Miyai et al. (2023b) to preprocess ImageNet22K and COCO data. We only evaluate the OOD datasets that have no overlapping categories as the ID dataset.

We provide more details about the datasets used in our experiments, in terms of data sources, preprocessing, and the statistics for each dataset, as shown in Table 9 and below.

ImageNet1K We use the ImageNet-1000 (ILSVRC2012) (Deng et al., 2009) dataset for ID validation and testing. The original dataset contains 1.2 million training images and 50,000 validation images from 1000 classes, and is widely used for image classification. We follow Ming et al. (2022) to construct the ImageNet1K ID test set from the validation set. Additionally, we curated an ImageNet1K ID validation set from the training set by randomly selecting one image for each label.

Pascal-VOC The Pascal VOC (Visual Object Classes) (Everingham et al., 2009) dataset is a benchmark dataset widely used in computer vision, featuring annotated images across multiple object categories. We use the Pascal-VOC subset collected by Miyai et al. (2023b) as the ID dataset, each image has single-class ID objects and one or more OOD objects. The ID validation and test set are split by 1:9 for each class, resulting in 94 and 906 images, respectively.

iNaturalist iNaturalist (Van Horn et al., 2018) is a biodiversity dataset containing millions of labeled images of plants, animals, and insects. Ming et al. (2022) construct a subset with 10,000 images by de-duplicating concepts overlapped with ID datasets.

Places Places (Zhou et al., 2017) is a scene-centric database with 205 scene categories and 2.5 million images. We use the SUN subset collected by Ming et al. (2022) as the OOD test set, which contains 10,000 images that are not overlapped with the ID classes.

SUN SUN (Scene UNDERstanding) (Xiao et al., 2010) is a comprehensive collection of labeled images representing a diverse range of indoor and outdoor scenes. We use the SUN subset collected by Ming et al. (2022) as the OOD test set, which contains 10,000 images that are not overlapped with the ID classes.

Texture The Texture dataset (DTD) (Cimpoi et al., 2014) comprises 5640 images categorized into 47 terms inspired by human perception, aimed at replicating human-like texture recognition in machines. Again, we use the subset collected by Ming et al. (2022) as the OOD test set.

ImageNet22K The ImageNet-22K dataset (Russakovsky et al., 2015), formerly known as ImageNet-21K, addresses the underestimation of its additional value compared to the standard ImageNet-1K

pretraining, aiming to provide high-quality pretraining for a broader range of models. We use the filtered subset collected by Wang et al. (2021) as the OOD test set for MC-COCO and Pascal-VOC ID test sets.

COCO Miyai et al. (2023b) curated an MS-COCO OOD test set (COCO for short) with 1,000 images that are not overlapped with the Pascal-VOC ID classes, which we use as OOD testing data for Pascal-VOC ID test set.

D Fine-tune Baselines

We compare SeTAR+FT with 4 finetuning-based baselines. These baselines include:

- **NPOS.** NPOS (Tao et al., 2023) generates virtual anomalies in low-probability regions of ID data without relying on distribution assumptions, enhancing discrimination during training.
- **CoOp.** CoOp (Zhou et al., 2022) optimizes prompts for vision-language models with learnable context vectors for efficient few-shot learning.
- **LoCoOp.** LoCoOp (Miyai et al., 2023a) improves upon CoOp by leveraging CLIP’s local features to better distinguish between ID and OOD samples, achieving higher detection accuracy with less training data. We follow the official code⁹ to prepare and fine-tune the LoCoOp with CLIP-base and CLIP-large. Follow Miyai et al. (2023a), the top-K, λ , learning rate and epoch num are set to 200, 0.25, 0.002 and 50. Temperature is set to 1 and the text prompt is initiated with “X X X X X X X X X X X X X X X [CLASS]”, where [CLASS] is the ID class name. We average the results from 3 seeds finetuned with 1-shot ImageNet1K valid data.
- **LoRA.** LoRA (Hu et al., 2022) is a low-rank adaptation method that injects trainable low-rank decomposition matrices into the pre-trained model to adapt to downstream tasks. We apply low-rank adaptation to the same weight type as SeTAR+FT, the rank of each layer is set to match the trainable parameters of SeTAR. Details settings can be found in Table 11.

E HyperParameters Settings

The hyperparameters for SeTAR are shown in Table 10. And the hyperparameters for SeTAR+FT and LoRA are shown in Table 11.

Table 10: **Hyperparameters for SeTAR .** Temperature is set to 1 except for Swin-base with Energy score, where it is set to 0.1.

Backbone	Dataset	λ	top-K
CLIP-base	ImageNet1K	0.10	300
	Pascal-VOC	0.05	4
CLIP-large	ImageNet1K	0.50	300
	Pascal-VOC	0.30	6
Swin-base	ImageNet1K	0.01	700

Table 11: **Hyperparameters for SeTAR+FT and LoRA on ImageNet1K.** Temperature is set to 1 except for Swin-base with Energy score, which is set to 0.1.

Backbone	λ	top-K	LR	Epoch	Rank for LoRA	Alpha for LoRA
CLIP-base	0.10	300	0.01	5	32	16
CLIP-large	0.50	300	0.01	5	64	16
Swin-base	0.01	700	0.01	5	112	16

⁹<https://github.com/AtsuMiyai/LoCoOp>

F More Detailed Experiment Results

In this section, we present additional detailed results from the main paper. This includes the detailed results of fine-tuned baselines on the ImageNet1K benchmark in Table 12; detailed ablation results on modality, W_p , λ , and top-K in Table 13, Table 14, Table 17, and Table 19; and detailed results of SeTAR with different search algorithms, prune strategies and backbones in Table 16, Table 18 and Table 15.

Table 12: **Detail results of FPR95(FPR) and AUROC(AUC) compared with fine-tuned baselines on ImageNet1K benchmark.** † is cited from Tao et al. (2023). * denotes the results of our re-run.

Method	iNaturalist		SUN		Places		Texture		Average	
	FPR↓	AUC↑	FPR↓	AUC↑	FPR↓	AUC↑	FPR↓	AUC↑	FPR↓	AUC↑
CLIP-base										
MCM Score										
NPOS†	19.59	95.68	48.26	89.70	49.82	88.77	51.12	87.58	42.20	90.43
CoOp†	43.38	91.26	38.53	91.95	46.68	89.09	50.64	87.83	44.81	90.03
LoCoOp†	38.49	92.49	33.27	93.67	39.23	91.07	49.25	89.13	40.17	91.53
LoCoOp*	31.33	93.64	33.68	93.37	42.31	90.10	51.72	87.75	39.76	91.22
LoRA*	30.50	94.51	35.08	92.87	43.20	90.03	57.91	85.97	41.67	90.85
SeTAR+FT	32.95	93.41	30.26	93.81	38.56	91.24	53.32	87.72	38.77	91.55
GL-MCM Score										
NPOS†	18.70	95.36	38.99	90.33	41.86	89.36	47.89	86.44	36.86	90.37
CoOp†	21.30	95.27	31.66	92.16	40.44	89.31	52.93	84.25	36.58	90.25
LoCoOp†	24.61	94.89	25.62	94.59	34.00	92.12	49.86	87.49	33.52	92.14
LoCoOp*	18.97	95.90	27.33	94.31	37.29	90.75	52.98	85.95	34.14	91.73
LoRA*	15.16	96.48	27.99	93.48	36.74	90.30	57.56	83.24	34.36	90.88
SeTAR+FT	21.62	95.43	23.38	94.89	32.60	91.93	51.18	87.01	32.19	92.31
CLIP-large										
MCM Score										
LoCoOp*	41.84	91.77	35.28	92.78	41.52	90.01	44.33	89.96	40.74	91.13
LoRA*	34.65	93.65	29.78	94.21	36.65	91.59	53.40	87.18	38.62	91.66
SeTAR+FT	22.41	95.83	40.07	91.98	45.19	90.13	31.37	93.48	34.75	92.86
GL-MCM Score										
LoCoOp*	51.56	89.45	37.85	92.43	43.86	89.33	53.72	86.05	46.74	89.32
LoRA*	41.00	91.96	31.69	93.85	39.65	90.79	61.22	82.46	43.39	89.76
SeTAR+FT	36.56	91.93	34.81	93.08	41.08	90.66	35.74	91.66	37.05	91.83
Swin-base										
MSP Score										
LoRA*	43.14	87.02	62.66	78.04	67.95	74.90	54.34	81.99	57.02	80.49
SeTAR+FT	29.10	94.38	52.39	86.75	57.67	85.80	49.31	84.28	47.12	87.80
Energy Score										
LoRA*	62.49	71.48	65.05	71.47	75.00	63.24	46.13	85.02	62.17	72.80
SeTAR+FT	29.76	91.56	42.76	87.06	51.73	82.85	32.90	90.56	39.29	88.01

Table 13: **Detail results of ablation study on modality.** We use CLIP-B/16 as a backbone.

Method	iNaturalist		SUN		Places		Texture		ImageNet22K		COCO		Average	
	FPR↓	AUC↑	FPR↓	AUC↑	FPR↓	AUC↑	FPR↓	AUC↑	FPR↓	AUC↑	FPR↓	AUC↑	FPR↓	AUC↑
ImageNet1K														
MCM Score														
Visual	29.69	94.58	35.15	92.99	41.25	90.45	55.00	86.92	-	-	-	-	40.27	91.24
Text	30.21	94.33	38.39	92.27	44.48	89.74	58.05	85.64	-	-	-	-	42.78	90.50
Visual+Text	26.92	94.67	35.57	92.79	42.64	90.16	55.83	86.58	-	-	-	-	40.24	91.05
GL-MCM Score														
Visual	13.81	96.93	27.89	93.67	36.12	90.74	54.06	85.06	-	-	-	-	32.97	91.60
Text	15.44	96.54	30.77	92.78	38.95	89.71	58.14	83.17	-	-	-	-	35.82	90.55
Visual+Text	13.36	96.92	28.17	93.36	36.80	90.40	54.17	84.59	-	-	-	-	33.12	91.32
Pascal-VOC														
MCM Score														
Visual	4.13	98.63	26.31	94.58	30.44	92.58	42.48	93.20	45.19	92.36	50.60	89.36	33.19	93.45
Text	7.29	98.06	26.33	94.68	30.25	92.65	44.57	92.25	44.38	92.40	48.00	90.45	33.47	93.42
Visual+Text	4.59	98.71	24.91	95.15	28.46	93.21	40.44	93.58	48.25	92.08	48.10	89.70	32.46	93.74
GL-MCM Score														
Visual	3.90	98.89	22.40	94.27	26.22	93.03	22.87	95.97	31.40	94.10	42.50	90.81	24.88	94.51
Text	3.55	99.01	21.26	94.48	24.87	92.96	30.89	94.07	29.86	94.49	37.10	92.09	24.59	94.52
Visual+Text	3.66	98.96	21.93	94.81	25.04	93.62	20.35	96.36	31.47	94.31	40.70	91.19	23.86	94.87

Table 14: **Detail results of SeTAR with and without considering projection matrix W_p .** We use CLIP-B/16 as a backbone.

Method	iNaturalist		SUN		Places		Texture		ImageNet22K		COCO		Average	
	FPR↓	AUC↑	FPR↓	AUC↑	FPR↓	AUC↑	FPR↓	AUC↑	FPR↓	AUC↑	FPR↓	AUC↑	FPR↓	AUC↑
ImageNet1K														
MCM Score														
Vanilla MCM	32.07	94.43	38.65	92.37	43.73	90.03	57.89	86.13	-	-	-	-	43.09	90.74
SeTAR w W_p	35.21	93.06	33.50	93.16	41.02	90.50	57.41	86.22	-	-	-	-	41.79	90.74
SeTAR w/o W_p	26.92	94.67	35.57	92.79	42.64	90.16	55.83	86.58	-	-	-	-	40.24	91.05
GL-MCM Score														
Vanilla GL-MCM	15.34	96.62	30.65	93.01	37.76	90.07	57.41	83.73	-	-	-	-	35.29	90.86
SeTAR w W_p	19.08	95.69	26.52	93.93	35.18	91.01	56.42	84.34	-	-	-	-	34.30	91.24
SeTAR w/o W_p	13.36	96.92	28.17	93.36	36.80	90.40	54.17	84.59	-	-	-	-	33.12	91.32
Pascal-VOC														
MCM Score														
Vanilla MCM	7.24	98.23	27.91	94.56	32.40	92.45	51.61	91.89	50.60	91.42	53.70	89.30	37.24	92.98
SeTAR w W_p	6.54	98.40	26.95	94.88	30.61	92.91	49.40	92.09	51.16	91.84	51.00	89.83	35.94	93.32
SeTAR w/o W_p	4.59	98.71	24.91	95.15	28.46	93.21	40.44	93.58	48.25	92.08	48.10	89.70	32.46	93.74
GL-MCM Score														
Vanilla GL-MCM	4.33	98.81	22.94	94.63	26.20	93.11	41.61	92.88	37.88	93.17	43.70	90.71	29.44	93.88
SeTAR w W_p	3.20	98.93	20.73	94.77	23.91	93.53	22.06	95.89	30.65	94.38	39.50	91.41	23.34	94.82
SeTAR w/o W_p	3.66	98.96	21.93	94.81	25.04	93.62	20.35	96.36	31.47	94.31	40.70	91.19	23.86	94.87

Table 15: **Detail results for SeTAR with different backbones.** * denotes the result of our re-run.

Method	iNaturalist		SUN		Places		Texture		ImageNet22K		COCO		Average	
	FPR↓	AUC↑	FPR↓	AUC↑	FPR↓	AUC↑	FPR↓	AUC↑	FPR↓	AUC↑	FPR↓	AUC↑	FPR↓	AUC↑
ImageNet1K														
CLIP-base														
Vanilla MCM*	32.07	94.43	38.65	92.37	43.73	90.03	57.89	86.13	-	-	-	-	43.09	90.74
SeTAR+MCM	26.92	94.67	35.57	92.79	42.64	90.16	55.83	86.58	-	-	-	-	40.24	91.05
Vanilla GL-MCM*	15.34	96.62	30.65	93.01	37.76	90.07	57.41	83.73	-	-	-	-	35.29	90.86
SeTAR+GL-MCM	13.36	96.92	28.17	93.36	36.80	90.40	54.17	84.59	-	-	-	-	33.12	91.32
CLIP-large														
Vanilla MCM*	28.17	94.97	29.18	94.12	33.66	92.37	57.73	85.46	-	-	-	-	37.19	91.73
SeTAR+MCM	26.96	95.14	27.12	94.54	32.04	92.55	58.90	85.45	-	-	-	-	36.26	91.92
Vanilla GL-MCM*	29.58	94.43	32.54	93.35	37.18	91.43	63.28	80.71	-	-	-	-	40.65	89.98
SeTAR+GL-MCM	30.96	94.04	28.72	94.08	34.58	91.89	63.90	80.89	-	-	-	-	39.54	90.22
SwinTransformerV2-base														
Vanilla MSP*	44.78	89.89	63.12	82.81	67.07	81.45	62.04	82.33	-	-	-	-	59.25	84.12
SeTAR+MSP	41.44	91.08	60.05	85.04	64.31	83.70	58.39	83.26	-	-	-	-	56.05	85.77
Vanilla Energy*	57.52	81.60	71.98	72.93	76.90	68.90	53.65	80.96	-	-	-	-	65.01	76.10
SeTAR+Energy	41.71	89.42	56.53	83.29	62.84	80.20	45.37	84.76	-	-	-	-	51.61	84.42
Pascal-VOC														
CLIP-base														
Vanilla MCM*	7.24	98.23	27.91	94.56	32.40	92.45	51.61	91.89	50.60	91.42	53.70	89.30	37.24	92.98
SeTAR+MCM	4.59	98.71	24.91	95.15	28.46	93.21	40.44	93.58	48.25	92.08	48.10	89.70	32.46	93.74
Vanilla GL-MCM*	4.33	98.81	22.94	94.63	26.20	93.11	41.61	92.88	37.88	93.17	43.70	90.71	29.44	93.88
SeTAR+GL-MCM	3.66	98.96	21.93	94.81	25.04	93.62	20.35	96.36	31.47	94.31	40.70	91.19	23.86	94.87
CLIP-large														
Vanilla MCM*	42.90	94.69	44.27	93.28	41.48	91.57	61.33	89.95	63.37	91.20	59.90	89.40	52.21	91.68
SeTAR+MCM	26.05	96.23	35.97	94.20	33.10	92.45	50.32	91.91	57.69	92.02	52.30	90.67	42.57	92.91
Vanilla GL-MCM*	23.29	96.17	40.76	93.49	41.23	91.69	54.98	89.60	53.19	92.67	50.30	91.09	43.96	92.45
SeTAR+GL-MCM	9.62	97.51	27.75	94.73	28.85	92.99	41.77	92.40	39.42	93.98	39.30	92.38	31.12	94.00

Table 16: **Detail results for different search algorithms.** Here LES stands for layer-exhaustive greedy search, MIS stands for modality-interleave greedy search, and SeTAR-S stands for the search algorithm of SeTAR, which searches vision and text layers sequentially. We use CLIP-B/16 as a backbone.

Method	iNaturalist		SUN		Places		Texture		ImageNet22K		COCO		Average	
	FPR↓	AUC↑	FPR↓	AUC↑	FPR↓	AUC↑	FPR↓	AUC↑	FPR↓	AUC↑	FPR↓	AUC↑	FPR↓	AUC↑
ImageNet1K														
MCM Score														
LES	30.25	94.26	36.42	92.79	42.97	90.15	58.33	85.89	-	-	-	-	41.99	90.78
MIS	28.63	94.46	35.41	92.80	42.37	90.17	55.78	86.59	-	-	-	-	40.55	91.00
SeTAR-S	26.92	94.67	35.57	92.79	42.64	90.16	55.83	86.58	-	-	-	-	40.24	91.05
GL-MCM Score														
LES	14.43	96.61	27.81	93.49	36.16	90.51	57.20	83.72	-	-	-	-	33.90	91.08
MIS	14.14	96.76	28.28	93.39	36.86	90.39	54.15	84.64	-	-	-	-	33.36	91.29
SeTAR-S	13.36	96.92	28.17	93.36	36.80	90.40	54.17	84.59	-	-	-	-	33.12	91.32
Pascal-VOC														
MCM Score														
LES	5.20	98.73	26.88	95.03	30.78	92.93	44.73	93.35	50.98	91.97	52.10	89.61	35.11	93.60
MIS	5.82	98.49	25.52	95.04	30.10	92.98	43.95	93.06	50.00	92.06	48.20	89.84	33.93	93.58
SeTAR-S	4.59	98.71	24.91	95.15	28.46	93.21	40.44	93.58	48.25	92.08	48.10	89.70	32.46	93.74
GL-MCM Score														
LES	3.89	98.87	21.56	94.56	24.70	93.32	23.35	95.80	32.99	93.82	40.40	91.03	24.48	94.57
MIS	3.53	98.95	20.87	94.77	24.30	93.47	19.91	96.24	29.59	94.40	39.00	91.21	22.87	94.84
SeTAR-S	3.66	98.96	21.93	94.81	25.04	93.62	20.35	96.36	31.47	94.31	40.70	91.19	23.86	94.87

Table 17: **Detail results of ablation study on λ .** We use CLIP-B/16 as a backbone.

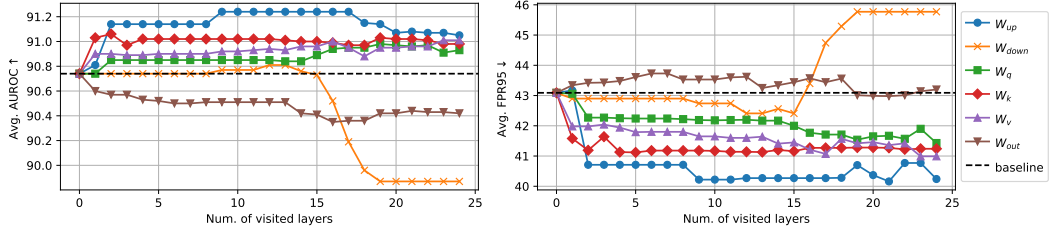
λ	iNaturalist		SUN		Places		Texture		ImageNet22K		COCO		Average	
	FPR↓	AUC↑	FPR↓	AUC↑	FPR↓	AUC↑	FPR↓	AUC↑	FPR↓	AUC↑	FPR↓	AUC↑	FPR↓	AUC↑
ImageNet1K														
MCM Score														
0.01	28.31	94.60	36.83	92.74	43.01	90.10	55.85	86.58	-	-	-	-	41.00	91.00
0.05	27.41	94.75	35.91	92.70	42.75	90.15	55.57	86.49	-	-	-	-	40.41	91.02
0.10	26.92	94.67	35.57	92.79	42.64	90.16	55.83	86.58	-	-	-	-	40.24	91.05
0.15	34.29	93.66	35.88	92.85	42.34	90.24	58.09	86.01	-	-	-	-	42.65	90.69
0.20	34.89	93.62	35.59	92.88	41.95	90.28	58.19	86.11	-	-	-	-	42.66	90.72
0.25	35.88	93.42	35.48	92.76	42.24	90.18	58.39	85.84	-	-	-	-	43.00	90.55
0.30	37.72	93.26	36.27	92.64	42.35	90.10	58.46	86.03	-	-	-	-	43.70	90.50
GL-MCM Score														
0.01	13.98	96.76	29.20	93.17	37.56	90.09	54.10	84.47	-	-	-	-	33.71	91.12
0.05	13.90	96.79	28.84	93.24	37.25	90.32	54.20	84.33	-	-	-	-	33.55	91.17
0.10	13.36	96.92	28.17	93.36	36.80	90.40	54.17	84.59	-	-	-	-	33.12	91.32
0.15	16.85	96.12	26.99	93.72	35.14	90.74	56.79	83.90	-	-	-	-	33.94	91.12
0.20	17.21	96.10	27.12	93.70	35.31	90.72	57.22	83.89	-	-	-	-	34.21	91.10
0.25	18.30	95.87	27.55	93.64	36.06	90.58	58.28	83.70	-	-	-	-	35.05	90.95
0.30	17.95	95.98	27.91	93.63	36.14	90.53	57.59	84.03	-	-	-	-	34.90	91.04
Pascal-VOC														
MCM Score														
0.01	5.58	98.43	25.14	94.94	29.13	93.01	40.41	93.35	47.85	92.12	49.60	89.37	32.95	93.54
0.05	4.59	98.71	24.91	95.15	28.46	93.21	40.44	93.58	48.25	92.08	48.10	89.70	32.46	93.74
0.10	5.44	98.50	24.97	95.06	29.60	93.01	42.55	93.26	48.69	92.28	47.80	89.82	33.18	93.65
0.15	5.97	98.53	26.50	95.07	30.88	93.05	46.22	92.94	50.99	92.07	49.80	89.80	35.06	93.58
0.20	6.11	98.53	26.18	95.08	30.53	93.06	45.43	93.06	50.68	92.16	49.40	89.82	34.72	93.62
0.25	6.41	98.43	26.19	94.99	31.24	92.89	47.36	92.72	50.41	92.13	50.20	89.74	35.30	93.48
0.30	6.81	98.34	26.98	94.80	32.13	92.65	48.67	92.52	50.53	92.14	51.10	89.77	36.04	93.37
GL-MCM Score														
0.01	4.42	98.83	22.72	94.73	25.93	93.51	22.07	96.22	32.62	94.27	43.50	90.91	25.21	94.74
0.05	3.66	98.96	21.93	94.81	25.04	93.62	20.35	96.36	31.47	94.31	40.70	91.19	23.86	94.87
0.10	3.79	98.94	21.40	94.76	25.05	93.49	20.74	96.29	30.42	94.48	40.00	91.20	23.57	94.86
0.15	3.50	98.98	20.83	94.84	24.34	93.55	20.57	96.20	29.84	94.42	38.50	91.25	22.93	94.87
0.20	3.50	98.94	20.72	94.74	24.13	93.48	19.95	96.28	29.22	94.46	38.60	91.19	22.69	94.85
0.25	4.14	98.96	21.54	94.85	25.37	93.54	23.37	96.14	32.18	94.51	40.30	91.44	24.48	94.90
0.30	4.15	98.90	21.40	94.63	25.16	93.33	23.01	96.03	31.02	94.44	38.90	91.40	23.94	94.79

Table 18: **Detail results on different pruning strategies.** We use CLIP-B/16 as a backbone.

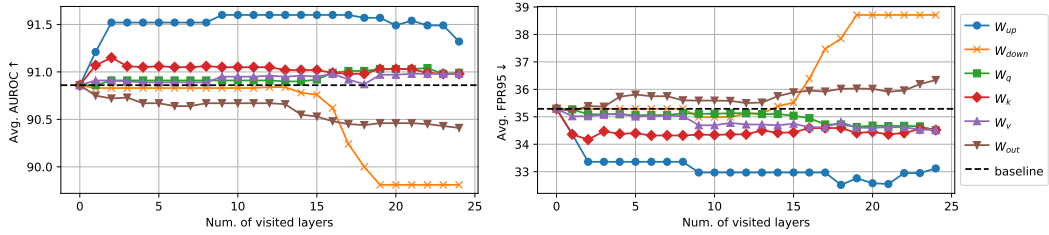
Method	iNaturalist		SUN		Places		Texture		ImageNet22K		COCO		Average	
	FPR↓	AUC↑	FPR↓	AUC↑	FPR↓	AUC↑	FPR↓	AUC↑	FPR↓	AUC↑	FPR↓	AUC↑	FPR↓	AUC↑
ImageNet1K														
MCM Score														
Principle	32.07	94.43	38.65	92.37	43.73	90.03	57.89	86.13	-	-	-	-	43.09	90.74
Random	32.07	94.43	38.65	92.37	43.73	90.03	57.89	86.13	-	-	-	-	43.09	90.74
Minor	26.92	94.67	35.57	92.79	42.64	90.16	55.83	86.58	-	-	-	-	40.24	91.05
GL-MCM Score														
Principle	15.34	96.62	30.65	93.01	37.76	90.07	57.41	83.73	-	-	-	-	35.29	90.86
Random	32.07	94.43	38.65	92.37	43.73	90.03	57.89	86.13	-	-	-	-	43.09	90.74
Minor	13.36	96.92	28.17	93.36	36.80	90.40	54.17	84.59	-	-	-	-	33.12	91.32
Pascal-VOC														
MCM Score														
Principle	9.91	98.01	29.24	93.91	32.89	92.30	54.43	90.30	53.53	91.07	49.20	89.07	38.20	92.44
Random	7.24	98.20	27.45	94.60	32.52	92.43	43.30	93.25	49.89	91.02	52.97	89.06	35.57	93.09
Minor	4.59	98.71	24.91	95.15	28.46	93.21	40.44	93.58	48.25	92.08	48.10	89.70	32.46	93.74
GL-MCM Score														
Principle	3.10	98.62	20.07	94.41	22.33	93.38	38.53	92.19	31.61	93.07	36.50	90.34	25.36	93.67
Random	3.47	98.99	20.04	95.46	24.07	93.95	31.76	94.86	35.71	93.67	42.17	91.04	26.20	94.66
Minor	3.66	98.96	21.93	94.81	25.04	93.62	20.35	96.36	31.47	94.31	40.70	91.19	23.86	94.87

Table 19: **Detail results of ablation study on top-K.** We use CLIP-B/16 as a backbone.

K	iNaturalist		SUN		Places		Texture		ImageNet22K		COCO		Average	
	FPR↓	AUC↑	FPR↓	AUC↑	FPR↓	AUC↑	FPR↓	AUC↑	FPR↓	AUC↑	FPR↓	AUC↑	FPR↓	AUC↑
ImageNet1K														
MCM Score														
0	26.50	94.70	36.22	92.66	43.04	90.10	55.82	86.46	-	-	-	-	40.39	90.98
100	26.92	94.67	35.57	92.79	42.64	90.16	55.83	86.58	-	-	-	-	40.24	91.05
200	26.92	94.67	35.57	92.79	42.64	90.16	55.83	86.58	-	-	-	-	40.24	91.05
300	26.92	94.67	35.57	92.79	42.64	90.16	55.83	86.58	-	-	-	-	40.24	91.05
400	26.92	94.67	35.57	92.79	42.64	90.16	55.83	86.58	-	-	-	-	40.24	91.05
500	26.92	94.67	35.57	92.79	42.64	90.16	55.83	86.58	-	-	-	-	40.24	91.05
600	26.50	94.70	36.22	92.66	43.04	90.10	55.82	86.46	-	-	-	-	40.39	90.98
700	26.92	94.67	35.57	92.79	42.64	90.16	55.83	86.58	-	-	-	-	40.24	91.05
800	26.92	94.67	35.57	92.79	42.64	90.16	55.83	86.58	-	-	-	-	40.24	91.05
900	29.38	94.38	36.02	92.75	42.47	90.24	55.20	86.77	-	-	-	-	40.77	91.03
1000	30.63	94.17	36.24	92.93	42.58	90.24	56.84	86.34	-	-	-	-	41.57	90.92
GL-MCM Score														
0	14.02	96.80	28.32	93.40	36.91	90.52	54.68	84.32	-	-	-	-	33.48	91.26
100	13.36	96.92	28.17	93.36	36.80	90.40	54.17	84.59	-	-	-	-	33.12	91.32
200	13.36	96.92	28.17	93.36	36.80	90.40	54.17	84.59	-	-	-	-	33.12	91.32
300	13.36	96.92	28.17	93.36	36.80	90.40	54.17	84.59	-	-	-	-	33.12	91.32
400	13.36	96.92	28.17	93.36	36.80	90.40	54.17	84.59	-	-	-	-	33.12	91.32
500	13.36	96.92	28.17	93.36	36.80	90.40	54.17	84.59	-	-	-	-	33.12	91.32
600	14.02	96.80	28.32	93.40	36.91	90.52	54.68	84.32	-	-	-	-	33.48	91.26
700	13.36	96.92	28.17	93.36	36.80	90.40	54.17	84.59	-	-	-	-	33.12	91.32
800	13.36	96.92	28.17	93.36	36.80	90.40	54.17	84.59	-	-	-	-	33.12	91.32
900	14.71	96.63	28.64	93.31	36.56	90.41	54.04	84.78	-	-	-	-	33.49	91.28
1000	15.82	96.42	28.61	93.46	37.20	90.40	54.75	84.35	-	-	-	-	34.10	91.16
Pascal-VOC														
MCM Score														
0	5.58	98.43	25.14	94.94	29.13	93.01	40.41	93.35	47.85	92.12	49.60	89.37	32.95	93.54
2	4.59	98.71	24.91	95.15	28.46	93.21	40.44	93.58	48.25	92.08	48.10	89.70	32.46	93.74
4	4.59	98.71	24.91	95.15	28.46	93.21	40.44	93.58	48.25	92.08	48.10	89.70	32.46	93.74
6	5.58	98.43	25.14	94.94	29.13	93.01	40.41	93.35	47.85	92.12	49.60	89.37	32.95	93.54
8	5.27	98.45	24.26	94.98	28.31	93.06	39.61	93.31	46.99	92.11	48.10	89.38	32.09	93.55
10	5.58	98.43	25.14	94.94	29.13	93.01	40.41	93.35	47.85	92.12	49.60	89.37	32.95	93.54
12	4.59	98.71	24.91	95.15	28.46	93.21	40.44	93.58	48.25	92.08	48.10	89.70	32.46	93.74
14	5.58	98.43	25.14	94.94	29.13	93.01	40.41	93.35	47.85	92.12	49.60	89.37	32.95	93.54
GL-MCM Score														
0	4.42	98.83	22.72	94.73	25.93	93.51	22.07	96.22	32.62	94.27	43.50	90.91	25.21	94.74
2	3.66	98.96	21.93	94.81	25.04	93.62	20.35	96.36	31.47	94.31	40.70	91.19	23.86	94.87
4	3.66	98.96	21.93	94.81	25.04	93.62	20.35	96.36	31.47	94.31	40.70	91.19	23.86	94.87
6	4.42	98.83	22.72	94.73	25.93	93.51	22.07	96.22	32.62	94.27	43.50	90.91	25.21	94.74
8	4.47	98.84	22.76	94.79	25.99	93.56	22.39	96.19	32.85	94.27	43.30	90.95	25.29	94.76
10	4.42	98.83	22.72	94.73	25.93	93.51	22.07	96.22	32.62	94.27	43.50	90.91	25.21	94.74
12	3.66	98.96	21.93	94.81	25.04	93.62	20.35	96.36	31.47	94.31	40.70	91.19	23.86	94.87
14	4.42	98.83	22.72	94.73	25.93	93.51	22.07	96.22	32.62	94.27	43.50	90.91	25.21	94.74

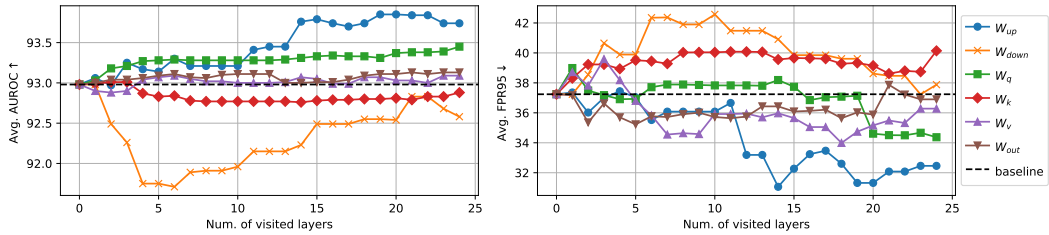


(a) MCM score

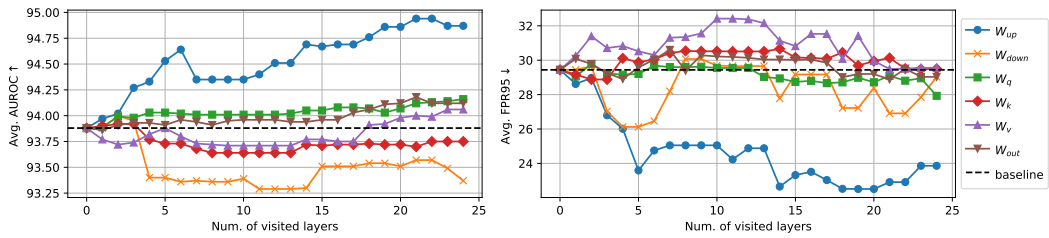


(b) GL-MCM score

Figure 2: Average AUROC/FPR95 of different weight types on ImageNet1K benchmark. We use CLIP-B/16 as a backbone.

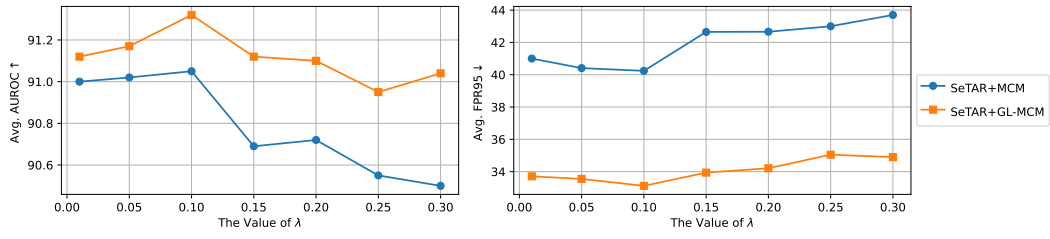


(a) MCM score

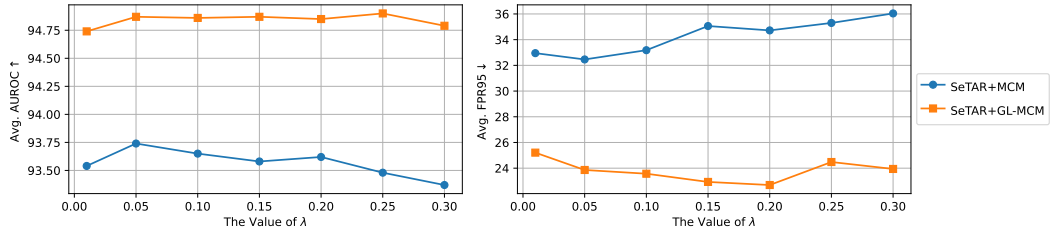


(b) GL-MCM score

Figure 3: Average AUROC/FPR95 of different weight types on Pascal-VOC benchmark. We use CLIP-B/16 as a backbone.

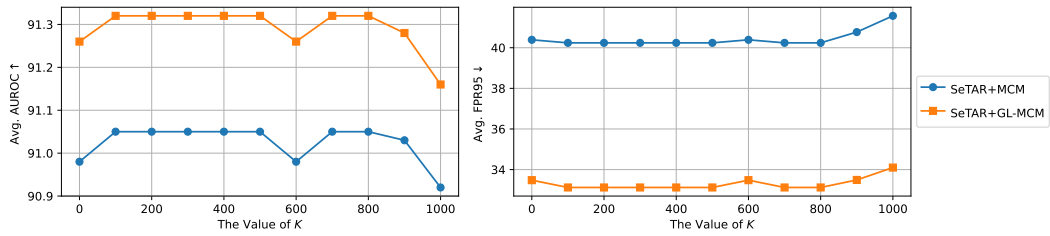


(a) ImageNet1K

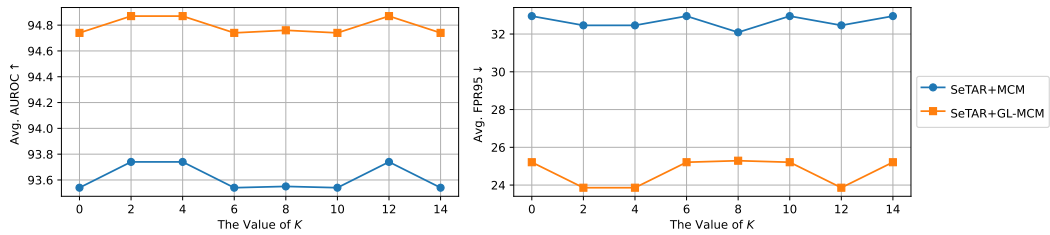


(b) Pascal-VOC

Figure 4: Ablation studies on λ on different ID datasets. We use CLIP-B/16 as a backbone.



(a) ImageNet1K



(b) Pascal-VOC

Figure 5: Ablation studies on top-K on different ID datasets. We use CLIP-B/16 as a backbone.

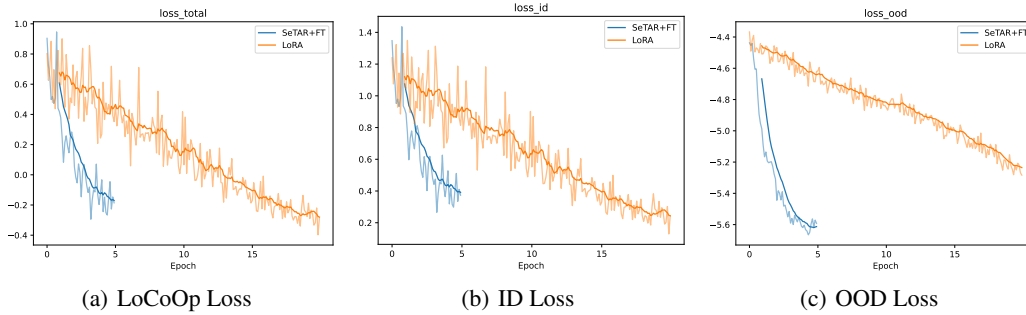


Figure 6: **Loss plots of SeTAR+FT v.s. LoRA on ImageNet1K.** We use CLIP-B/16 as a backbone. SeTAR+FT demonstrates faster convergence across all losses, especially in the OOD loss. For reference, with MCM score, SeTAR+FT achieves an average FPR of 38.77 at epoch 5. While LoRA achieves an average FPR of 42.88, 39.92 and 42.23 at epoch 1, 5 and 15, respectively.

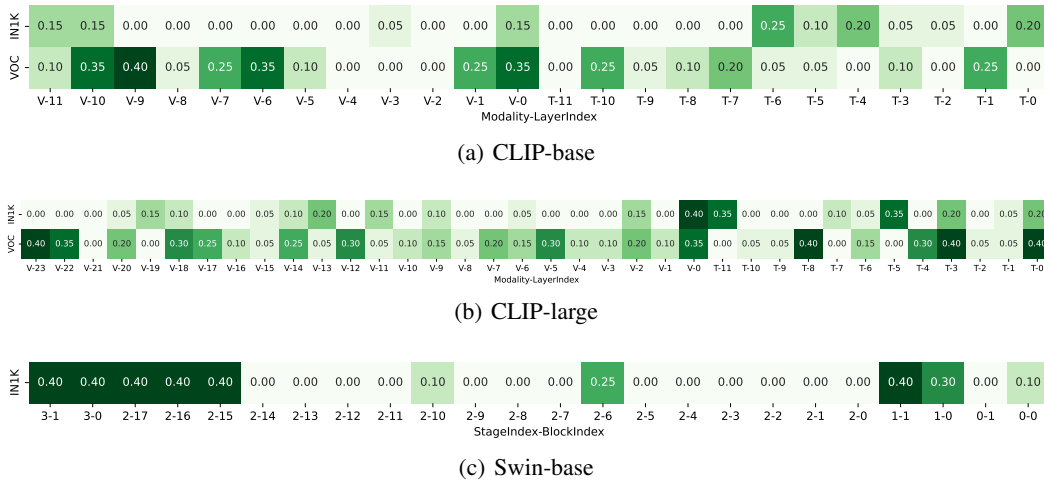


Figure 7: **Visualization of SeTAR rank reduction ratio distribution on different ID datasets with different backbones.** IN1K, VOC stand for ImageNet1K and Pascal-VOC. And V, T stand for visual modality and text modality of the CLIP model.

step	tower_type	weight_type	layer_num	best_ratio	total_loss*	id_loss	ood_loss	val_acc	ood_patch_percent
0	visual	W_up	11	0.15	0.647777	1.093326	-4.455494	71.399998	38.906631
1	visual	W_up	10	0.15	0.644654	1.083629	-4.389751	71.799998	39.293876
2	visual	W_up	9	0.00	0.644654	1.083629	-4.389751	71.799998	39.293876
3	visual	W_up	8	0.00	0.644654	1.083629	-4.389751	71.799998	39.293876
4	visual	W_up	7	0.00	0.644654	1.083629	-4.389751	71.799998	39.293876
5	visual	W_up	6	0.00	0.644654	1.083629	-4.389751	71.799998	39.293876
6	visual	W_up	5	0.00	0.644654	1.083629	-4.389751	71.799998	39.293876
7	visual	W_up	4	0.00	0.644654	1.083629	-4.389751	71.799998	39.293876
8	visual	W_up	3	0.05	0.640844	1.079729	-4.388844	71.999998	39.209695
9	visual	W_up	2	0.00	0.640844	1.079729	-4.388844	71.999998	39.209695
10	visual	W_up	1	0.00	0.640844	1.079729	-4.388844	71.999998	39.209695
11	visual	W_up	0	0.15	0.640132	1.079109	-4.389775	72.199998	39.156123
12	text	W_up	11	0.00	0.640132	1.079109	-4.389775	72.199998	39.156123
13	text	W_up	10	0.00	0.640132	1.079109	-4.389775	72.199998	39.156123
14	text	W_up	9	0.00	0.640132	1.079109	-4.389775	72.199998	39.156123
15	text	W_up	8	0.00	0.640132	1.079109	-4.389775	72.199998	39.156123
16	text	W_up	7	0.00	0.640132	1.079109	-4.389775	72.199998	39.156123
17	text	W_up	6	0.25	0.630751	1.075123	-4.443716	71.600001	38.808673
18	text	W_up	5	0.10	0.630514	1.078703	-4.481889	71.599997	38.246428
19	text	W_up	4	0.20	0.622065	1.075958	-4.538932	72.000001	38.452552
20	text	W_up	3	0.05	0.620440	1.079326	-4.588857	71.999997	38.649488
21	text	W_up	2	0.05	0.618521	1.076858	-4.583368	71.600001	38.444899
22	text	W_up	1	0.00	0.618521	1.076858	-4.583368	71.600001	38.444899
23	text	W_up	0	0.20	0.615174	1.069851	-4.546776	72.499997	38.642345

Listing 1: Example procedure of SeTAR on ImageNet1K with CLIP-base. We search the visual and text tower from top to bottom. At each step, we select the best ratio that minimizes the loss.